Magnetic Resonance in Medicine 52:559–565 (2004)

Analysis of Noise Effects on DTI-Based Tractography Using the Brute-Force and Multi-ROI Approach

Hao Huang,[1,2] Jiangyang Zhang,[1,2] Peter C.M. van Zijl,[1,3] and Susumu Mori[1,3*]

Diffusion tensor tractography based on line propagation is a promising and widely used technique, but it is known to be sensitive to noise and the size and location of the seed regions of interest (ROIs). The effects of these parameters on the tractography results were analyzed quantitatively using high-resolution diffusion tensor imaging (DTI) with a high signal-to-noise ratio (SNR) on a fixed mouse brain. The anterior commissure (AC), as judged from a T_2-weighted image, was used as an anatomical reference within which the tracts could be located. Monte Carlo simulation was performed by adding Gaussian noise to the time domain data and repeating the tractography. Deviations of the tracking results were measured as a function of SNR. Such noise effects were evaluated for a simple one-ROI approach and a combined two-ROI and brute-force (BF) approach. The influence of ROI size and location for the two-ROI + BF approach was also analyzed. The results confirmed the hypothesis that one can increase the validity of DTI-based tractography by adopting the BF and multi-ROI approach, with respect to the simple one-ROI approach. Magn Reson Med 52: 559–565, 2004. © 2004 Wiley-Liss, Inc.

Key words: diffusion tensor imaging; tractography; noise analysis; brute-force and multi-ROI approach; brain

Diffusion tensor imaging (DTI) is an MR technique that can measure anisotropy of water diffusion inside the brain (1). This technique has shown that many regions of brain white matter have high diffusion anisotropy, which is attributed to the coherent structure of axonal tracts (2–9), i.e., water molecules tend to diffuse along axonal fibers. It has been shown that 3D fiber architecture can be estimated with the use of this fiber-orientation information (10–18). While several estimation methods have been proposed by different groups, one of the most popular methods is a simple approach whereby a line is propagated from a seed pixel based on the fiber-orientation information (10–14,16,18–20). The most common way to use this technique is to manually define a region of interest (ROI) based on an anatomical landmark, and then propagate lines from the group of pixels defined by the ROI. Figure 1 shows a schematic diagram of a line-propagation method (10,11). In Fig. 1a, an ROI (one pixel) is indicated by a bold box, which is also a seed pixel (shaded pixel). Because the seed and ROI consist of one pixel, only one line is propagated, showing one possible path of axonal bundles. Figure 1b and c show examples in which the seed pixel and the pixels defined by the ROI are not identical. This example shows that the seed pixel and the ROI do not always have to be the same to obtain similar results. If all pixels in the image are explored for line propagation, it is possible that there are many other seed pixels from which the tracking leads to the ROI (Fig. 1b and c). This method, hereafter called the brute-force (BF) approach, is not confined to the relationship of one propagation line per pixel in the ROI. Thus it has the potential to reveal a more comprehensive view of axonal tracts (including branching/merging of tracts) that are related to the ROI (16,21,22). Examples of actual reconstruction in a fixed mouse brain are shown in Fig. 1d and e for non-BF and BF approaches, respectively. Another widely used approach is the multi-ROI technique (16,21,23,24). In this approach, propagation results that penetrate at least two ROIs are searched. Again, the seed pixels can be the same as the defined ROIs. One can also combine the multi-ROI technique with the BF approach to find multiple lines that connect the ROIs.

One of the problems of tractography is that the results are prone to errors due to noise and partial volume effects. Probabilistic studies, in which results from many individuals are averaged, may ameliorate this shortcoming but they may not be suitable for single-subject studies, such as those required for clinical diagnoses (23,25–28). Several previous papers have discussed the validation of DTI and the effect of noise (20,29–31) based on simple line propagation from seed pixels. The purpose of the present study was to test the hypothesis that the combined multi-ROI and BF approach would be more robust against errors than the simple one-ROI approach. The multi-ROI approach is based on existing anatomical knowledge of tract trajectories, and imposes a strong constraint on propagation results. If a propagated line deviates from its real path by an error, it is highly unlikely that the deviating line would happen to return to the real path in the vast 3D space and penetrate the second ROI. By combining multi-ROI approach with the BF method, one can search pixels in the entire brain to find lines that connect the ROIs. Because the propagation tends to accumulate noise and partial volume errors, pixels in between the two ROIs will be the seed pixels that lead to the correct path with the minimum accumulation of errors.

To test the noise sensitivity with minimized partial volume effects, we performed DTI with a high signal-to-noise ratio (SNR) and high spatial resolution using a fixed mouse brain. The anterior commissure (AC) was used as a regional standard because its trajectory is anatomically well characterized, it isolated from other white matter tracts, and it can be readily defined with the use of a coregistered

[1]Department of Radiology, Division of MRI Research, Johns Hopkins University School of Medicine, Baltimore, Maryland.

[2]Department of Biomedical Engineering, Johns Hopkins University School of Medicine, Baltimore, Maryland.

[3]F.M. Kirby Research Center for Functional Brain Imaging, Kennedy Krieger Institute, Baltimore, Maryland.

Grant sponsor: NIH; Grant numbers: R01 AGZ0012, P41 R15241 and R21-EB000991.

*Correspondence to: Susumu Mori, Ph.D., Department of Radiology, Johns Hopkins University School of Medicine, 217 Traylor Bldg., 720 Rutland Ave., Baltimore, MD 21205. E-mail: Susumu@mri.jhu.edu

Received 5 November 2003; revised 30 January 2004; accepted 30 January 2004.

DOI 10.1002/mrm.20147
Published online in Wiley InterScience (www.interscience.wiley.com).

© 2004 Wiley-Liss, Inc.

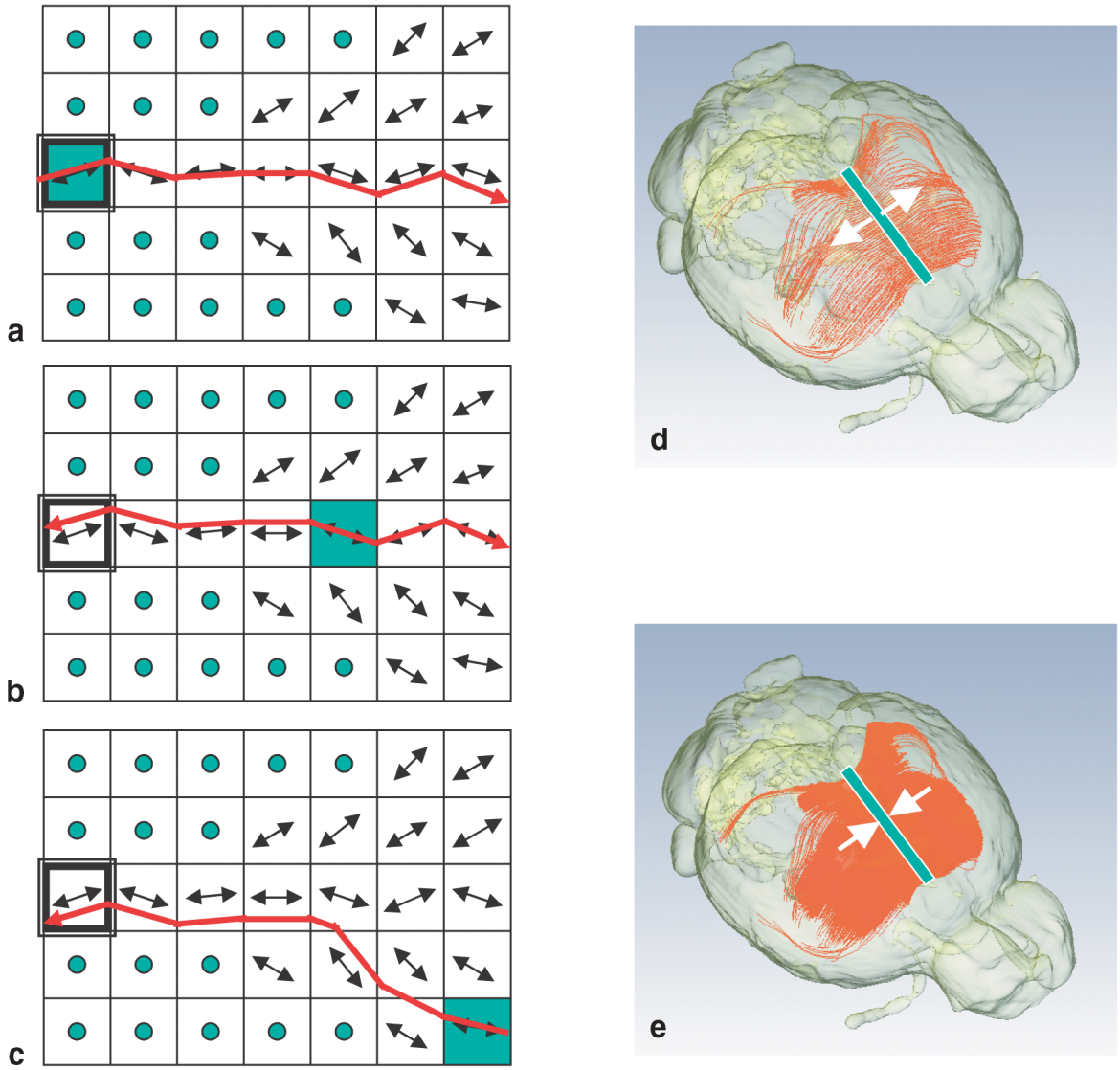

FIG. 1. Schematic diagrams of the hypothetical relationship between ROIs (double-line box) and seed pixels (shaded). **a:** The ROI and seed pixels are identical. Only one line is propagated. **b** and **c:** The ROI and seed pixels are not identical. Propagated lines from two different seed pixels reach the ROI, possibly delineating merging/branching patterns. **d** and **e:** Actual examples of tracking from the ROI (green bar in **d**) and to the ROI (green bar in **e**) for the corpus callosum. The white arrows in d and e indicate the tracking directions.

T_2-weighted image. We performed a Monte Carlo simulation by adding Gaussian noise to the time domain data and repeating the tractography. We then evaluated the effects of the noise for the simple one-ROI approach and the two-ROI + BF approach.

MATERIALS AND METHODS

Brain Preparation

In this study we used a male adult mouse (C57BL/6J) following a protocol approved by the Johns Hopkins Animal Care and Use Committee. The mouse was anesthetized with pentobarbital, and the brain was fixed by transcardiac perfusion with 4% paraformaldehyde in phosphate-buffered saline (PBS). The brain was dissected from the cranium and stored in a fixation solution for more than 2 weeks.

MRI

The mouse brain was placed in PBS for >24 hr before it was imaged. It was transferred into an in-house-built plastic MR-compatible tube. Inside the tube, the fixed mouse brain was immersed in fomblin buffer solution (Fomblin Profludropolyether; Ausimont, Thorofare, NJ) to keep the brain from dehydrating. A custom-made solenoid volume coil was used as both the RF coil and the signal receiver. The mouse brain was scanned with a GE Omega 400 (9.4T) spectrometer with a tri-axis gradient set. A diffusion-weighted spin-echo sequence with four echoes was used: the first two echoes were for imaging, and the last two served as navigators to monitor eddy-current-related phase errors and time-dependent signal instability. A set of diffusion-weighted (DW) images was acquired in 12 linearly independent directions: (0.699, 0.699, 0.152), (0.699,

0.152, 0.699), (0.152, 0.699, 0.699), (−0.699, 0.699, 0.152), (−0.699, 0.152, 0.699), (0.152, 0.699, −0.699), (−0.699, 0.152, −0.699), (0.699, 0.152, −0.699), (0.577, 0.577, 0.577), (−0.577, 0.577, 0.577), (−0.577, 0.577, −0.577), and (0.577, 0.577, −0.577) for (*Gx*, *Gy*, *Gz*) combinations, where *Gx* is the readout gradient, *Gy* is the phase-encoding I gradient, and *Gz* is the phase-encoding II gradient. In addition, two sets of data were acquired with minimal diffusion sensitization. In total, 14 images were acquired. The diffusion gradient strength was toggled between 23, 23, and 5 G/cm, and 18, 18, and 18 G/cm. The trapezoidal diffusion gradients had a duration of 3 ms with a rise time of 0.6 ms, and two bipolar gradients were separated by 3.8 ms. The minimum *b*-value was 150 s/mm^2, and the maximum *b*-value was 1000–1200 s/mm^2. To create an anatomical reference, we also acquired coregistered 3D T_2-weighted images. For DTI, a TR of 0.9 s, a TE of 33 ms, and two signal averages were used, for a total imaging time of 24 hr. For T_2-weighted imaging, we used TR = 2 s, TE = 80 ms, and two signal averages, for a total imaging time of 11 hr. The DTI matrix was 128 × 84 × 64, which was zero-filled to 256 × 168 × 128. The field of view (FOV) was 17 × 10.5 × 8 mm. Before zero-filling was performed, the nominal resolution was 132.8 × 125.0 × 125.0 μm. The imaging matrix of T_2 was 256 × 104 × 96, which was zero-filled to 512 × 209 × 192. The nominal resolution for T_2 before zero-filling was performed was 66.4 × 101.0 × 83.3 μm. The FOV was the same as that obtained with DTI.

Data Processing

All of the data processing was performed with the use of in-house-made software written in IDL (Iterative Data Language; Research Systems Inc., Boulder, CO). After the acquisition was performed, the raw data were separated into four blocks for the four echoes. We processed the first two blocks separately, utilizing the information provided by navigator echoes (last two blocks) for phase correction and gain calibration. The first navigator echo was used for phase correction of the first imaging echo, and the second navigator was used for the second block. After fast Fourier transform (FFT) of the individual blocks was performed, we obtained two magnitude images, which were added together for the SNR enhancement.

We calculated the DT using a multivariate linear fitting method, which resulted in three pairs of eigenvalues and eigenvectors for each pixel. The eigenvector (v1) associated with the largest eigenvalue (λ1) was assumed to represent the direction of the local axonal fiber. We used fractional anisotropy (FA) to quantify the anisotropy (32).

Noise Generation

In this study, the acquired high-resolution images were regarded as the "original" data, which had high SNR. To calculate the SNR, we obtained the background noise levels by measuring the root-mean-squared (RMS) signal intensity in regions of the images that contained no tissue. We estimated the signal by calculating the mean intensity in the regions where the intensity was higher than the noise level. For 14 images, the raw-data mean SNR was 65.

To analyze the effect of noise on DTI-based fiber tractography, we simulated thermal noise in an MR experiment

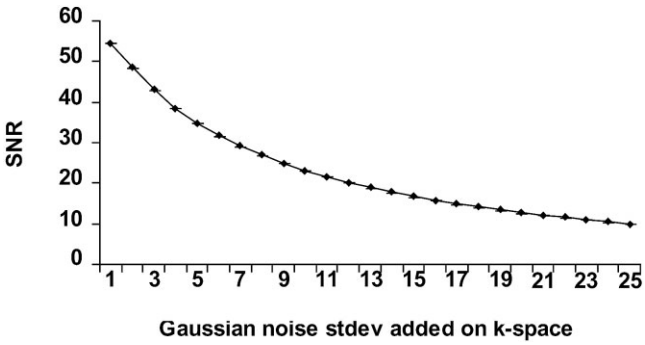

FIG. 2. Relationship between the SNR and Gaussian noise RMS used in this study.

with different RMS noise levels. Three groups of Gaussian noise were generated and added to the real and imaginary channels of the *k*-space raw data of 14 images. The groups were independent of each other. Each group contained 28 independent sets of Gaussian noise. Every two independent sets of Gaussian noise were for one of 14 images. To make the Gaussian noise independent among the three groups, and independent within each group, we randomly selected three large primary numbers as the seeds for three sets of normalized random values. Each set of normalized random values included 28 randomized values. Of these 28 values, 14 were used as seeds to generate Gaussian noise for the real channel of *k*-space raw data, and the other 14 were used as seeds to generate Gaussian noise for the imaginary channel of *k*-space raw data. The Gaussian noise was generated by means of the Box-Muller method. All of the Gaussian noises had a mean of 0 and a standard deviation (SD) of 1. After each Gaussian noise was scaled to 25 RMS noise level, it was added to the real or imaginary channel of *k*-space. With the FFT of noisy *k*-space raw data, we generated the amplitude raw data. We verified that the RMS of the noisy amplitude signal equaled the selected RMS noise level. With the same method we used to calculate the raw-data SNR, we calculated the mean SNR for 14 images at different noise levels. The relationship between the mean of the SNR and the Gaussian noise RMS (RMS noise level) is shown in Fig. 2. The figure shows that with a Gaussian noise RMS of 1–25, the corresponding SNR ranges from 10 to 60, which simulates the most common MR experimental circumstances. Thus, after noise was generated, three groups of noisy data sets (a total of 75 data sets) were created. Each group of noisy data sets had 25 noise levels, and each data set included a complete set of simulated DT images (14 images in this experiment).

Anatomical Reference and ROIs

Our reference white matter tissue boundary was hand-segmented from the coregistered T_2-weighted images. We chose the anterior part of the AC because it is well isolated from other white matter tracts, anatomically well documented, and easily defined from T_2-weighted images (Fig. 3a). Figure 3b shows the 3D reconstruction. Once the AC was defined, ROI #1 for DTI was fixed in an anterior coronal plane before the AC started to branch into the nose bulbs. ROI #2 was placed in a coronal plane anterior to the branching point of the anterior and posterior parts of the

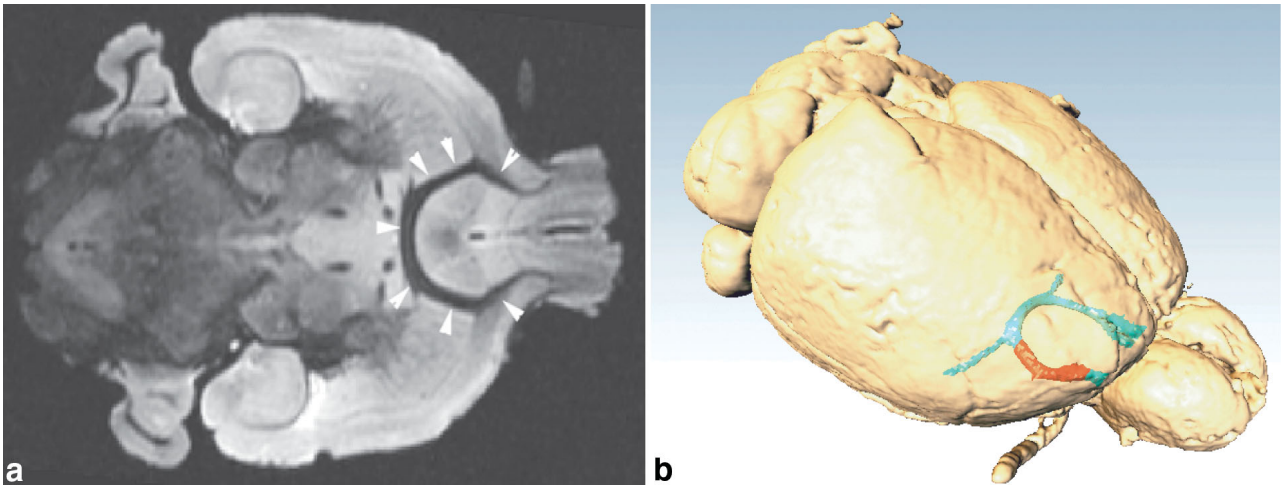

FIG. 3. T_2-weighted image (**a**) and 3D volume rendering (**b**) of the rat brain. The anterior part of the AC can be clearly identified in the T_2-weighted image (white arrowheads) and is well isolated from other white matter tracts. It is straightforward to manually delineate its trajectories, which are shown in part **b** (indicated by blue). A part of the AC (colored orange) was used as an anatomical reference for tractography.

AC. ROI #1 was anterior to ROI #2. Most of our analysis was performed in a region between these two ROIs (indicated by the orange color in Fig. 3b). As discussed in the Results section, we also studied the effect of ROI sizes (by dilating the two ROIs by three or five pixels) and the relative locations of ROI #2.

Tracking

The fiber tracking was based on a linear propagation model fiber assignment by continuous tracking (FACT) (10,11). Briefly, a line is propagated in both the orthograde (forward) and retrograde (backward) direction from the center of a seed pixel along the direction of eigenvector ($\underline{v1}$) of $\lambda 1$ (Fig. 1). In this approach, the starting point in the next pixel is the intercept of the previous pixel. For the termination, thresholds for anisotropy (e.g., FA $>$ 0.2) and angles between two vectors of connected pixels are often used. To minimize the effects of these arbitrary thresholds, we either did not employ them (propagation continues until it exits the brain) or we used only a low orientation threshold ($\underline{v1}_i \cdot \underline{v1}_j > 0.5$) to prevent sharp kinks. This latter termination criterion (hereafter called the orientation threshold) is based on the assumption that such sharp turns indicate that pixel resolution is not high enough to follow the trajectory curvature.

We used a conventional one-ROI approach and the two-ROI and BF approach to trace the trajectories with the three groups of simulated noisy data (a total of 75 datasets). For the one-ROI approach, tracking was initiated from ROI #1 (17 pixels), meaning that there were 17 seed pixels. For the two-ROI + BF approach, the second ROI #2 (35 pixels) was defined. Tracking was initiated from every other pixel in the image space (undersampled to one seed point per eight pixels to save computation time), and fiber trajectories that penetrated both ROI #1 and ROI #2 were selected as the reconstructed fibers. The number of tracked fibers was counted for the two-ROI + BF approach. Processing ruled out redundant fibers that had the same corresponding coordinates.

RESULTS

In the one-ROI approach, propagated lines are always 17 tracts (the size of ROI #1) regardless of SNR. However, in the two-ROI + BF approach, the number of propagated lines that penetrate both ROIs depends strongly on the SNR. This is illustrated in Fig. 4, which shows that the number of lines decreases as the SNR goes down. We defined a traced fiber as "valid" if it lay completely inside the AC defined by T_2-weighted images. We then counted the number of valid fibers over the number of all of the traced fibers. The result is also shown in Fig. 4. The number of nonvalid lines (false results) increased when SNR

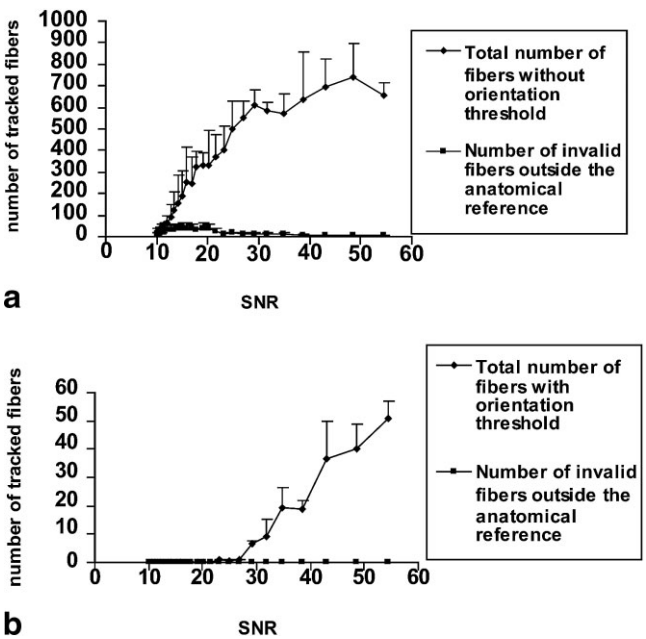

FIG. 4. Number of tracked fibers with different SNRs by the two-ROI + BF approach (**a**) without and (**b**) with an orientation threshold. The RMS was calculated from three trials of noise generation.

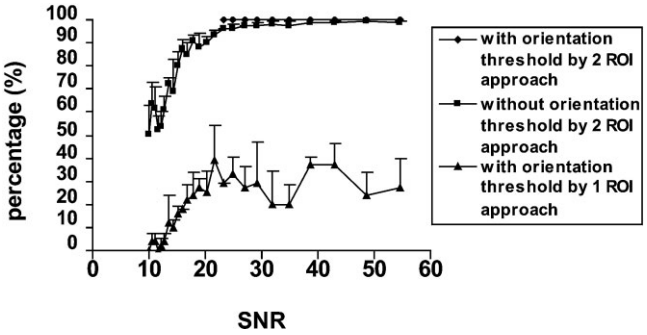

FIG. 5. Ratio of valid fibers as a function of SNR. The RMS was calculated from three trials of noise generation.

became lower than 20 (Fig. 4a). By applying an angle threshold of 0.5 (no more than 60° turns), no tracking results were found that penetrated both ROIs with SNR $<$ 23, and no false results were found (Fig. 4b).

Figure 5 shows the relationship between the valid fiber percentage and SNR for the two-ROI + BF approach with and without an orientation threshold, and for the one-ROI approach with an orientation threshold. As can be deduced from Fig. 4, the two-ROI + BF approach with orientation threshold yielded a 100% validity that was independent of SNR. Without the orientation threshold, the validity began to deteriorate for SNR values $<$ 20. For the one-ROI approach, four to seven tracking results from the 17 seed pixels stayed within the AC (24–41%) if the SNR was $\geq$ 20, but the percentage of valid fiber precipitates with the lower SNR.

Figure 6 shows tracking results obtained when the sizes of both ROIs were dilated by five pixels for the two-ROI + BF approach. When these data are compared with Fig. 4b, it can be seen that the effect is minimal (i.e., all tracts that were found to penetrate both ROIs were 100% within the AC). Again, noise affected the number of lines but not the validity. This figure implies that the tracking results from the two-ROI + BF approach are less sensitive to the change of ROI sizes compared to the one-ROI approach.

Figure 7a shows 3D reconstruction results when ROI #2 was moved to the anterior part of the AC of the opposite hemisphere. The effects of noise for this set of ROIs are shown in Fig. 7b. For comparison, results from the original set of ROIs are also shown. Again, as long as the lines between the two ROIs can be traced out, they are all within the AC. There are less lines than in the original ROI set because there is more distance between the two ROIs.

DISCUSSION

The DTI-based fiber reconstruction technique has the potential to reveal brain axonal architectures, which no other imaging tools can obtain noninvasively. However, this technique has many known limitations. First, the low imaging resolution of MRI (typically 1–5 mm for human studies) allows us to study only large bundles of axons with uniform orientation. Second, the tensor-based calculation assumes that there is no curvature or mixture of fiber orientation within a pixel, which is often not the case. Third, the reconstruction results are sensitive to noise, partial volume effects, and selection of seed pixels. These limitations are often fundamental and can not be completely eliminated. Thus, tractography with the current experimental constraints is at best an approximation tool to decipher the complicated brain axonal architecture. However, if we understand these limitations and use the tool in a proper manner, there is a great potential that it will provide us with important and unique information regarding the anatomy of the brain.

In this study, we assessed the effects of noise on tractography and compared the results for one-ROI and two-ROI + BF approaches. We used the AC defined by a T_2-weighted image as an outer-boundary reference within which tracking results were assumed to be "valid." Although this standard agrees well with the classical definition of the AC by histology, and we are comfortable with our assumption, there are several important factors that should be considered. First, if a tracking result deviates from our anatomical reference, we can not declare the result to be "false." For example, even with the highest SNR, more than 50% of the one-ROI results deviated from our anatomical reference. This may be due to the limitations of DTI (error) or it may reflect a true branching of the AC, which we can not judge. Second, we can not generalize our finding regarding validity using the AC. For example, the two-ROI + BF approach achieved 100% validity in our study regardless of SNR. However, this does not mean that tracking results obtained with this approach are always valid. The AC is well isolated from other white matter tracts, and it does not have complex spatial interactions with other tracts. This tract is also one of the largest tracts in the mouse brain. If imaging resolution is much lower, or the tract of interest is much narrower, validity may vary. Therefore, our results reveal only general properties of the two-ROI + BF approach with respect to the more simple and widely-used one-ROI approach: the results from the two-ROI + BF approach are more stable against noise, and the validity of the two-ROI + BF approach for tracing known trajectories (defined by the two ROIs) is high. The effect of noise is the reduction of the number of lines found to penetrate the two ROIs while the validity and reproducibility of the tract trajectory was high in this study.

One drawback of the two-ROI + BF approach is that with this method one can study only trajectories of known

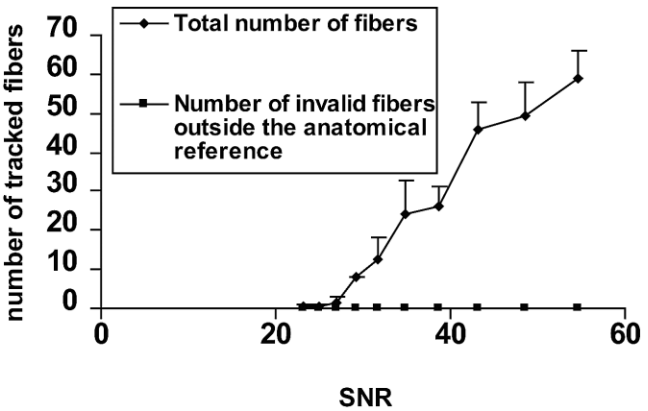

FIG. 6. Number of tracked fibers with both ROIs dilated by five pixels using the two-ROI and BF approach with an orientation threshold. The RMS was calculated from three trials of noise generation.

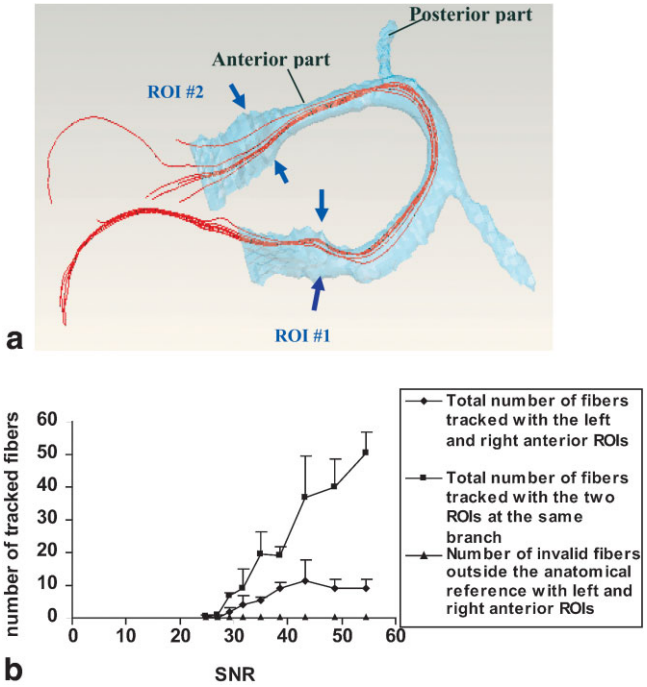

FIG. 7. Locations of two ROIs (**a**), and the tracking results and effects of noise (**b**). In this trial, ROI #2 was moved to the opposite hemisphere to reveal the entire trajectory of the anterior part of the AC. The surface rendering (blue) is T_2-defined AC, and the red lines indicate reconstruction results.

white matter tracts, and one can not examine branching in between the two ROIs. A good example is shown in Fig. 7a. Only the anterior part of the AC is traced with the constraints of two ROIs both placed at anterior parts of the AC, while the tracking results of a true branching in the posterior part can not be reconstructed.

It should be noted that the tracking results visualized in Fig. 7 represent only a portion of the AC defined by T_2-weighted imaging. As a related issue, it would be interesting to determine whether one could use tractography to estimate the volume of the tract by counting the number of pixels it penetrates. However, we encountered several difficulties when we attempted to validate the tract volume measurement using the present model. The first difficulty was related to the true definition of the tract. The T_2-defined AC was used as a standard for the spatial extent of the trajectory in this study, but not for the volume. The AC boundary in the T_2-weighted images was defined by an arbitrary intensity threshold, and the AC volume varied depending on the threshold. The AC also consists of axons that connect different areas of the brain. Most notably, it has posterior and anterior branches, as indicated in Fig. 7. The tractography result shown in Fig. 7 reconstructs a path that connects only the anterior branches of the two hemispheres, which does not contain posterior–posterior and anterior–posterior connections as the T_2-defined AC should. Therefore, a volume difference between the T_2-defined AC and the tractography-defined AC was expected. The second difficulty is related to reproducibility, because the number of reconstructed lines is sensitive to the SNR. Therefore, the SNR must be comparable

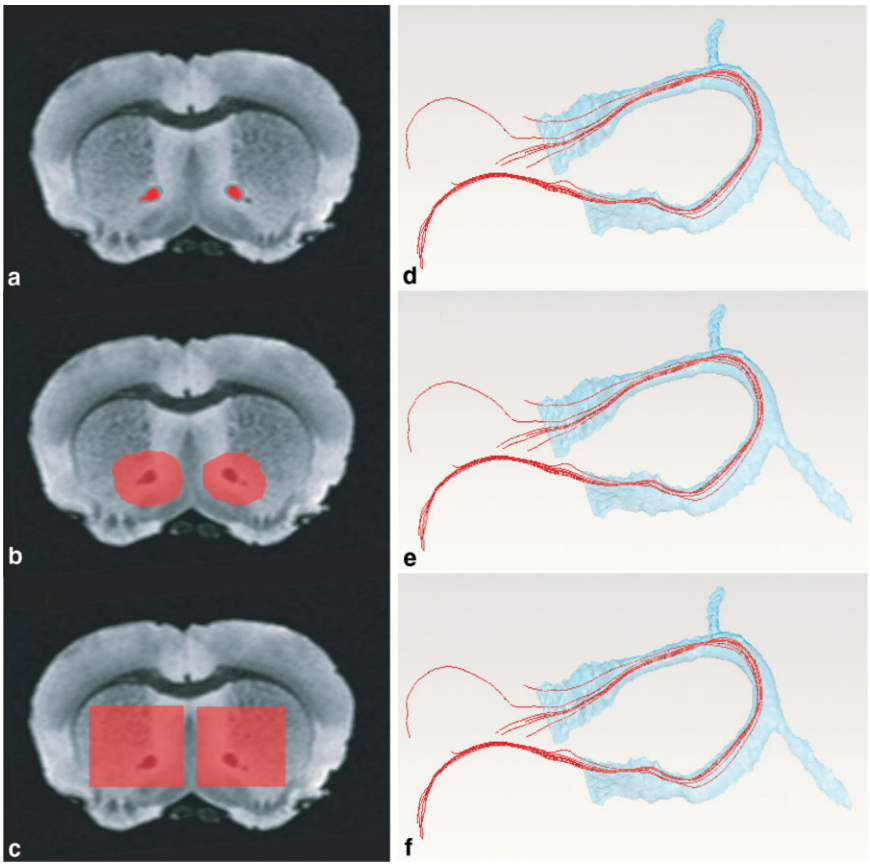

FIG. 8. Demonstration of low sensitivity to ROI drawing when the two-ROI + BF approach is used. Placing the ROIs with different shapes and sizes, indicated by red shaded regions in **a–c**, results in the same tracking results (**d–f**).

among samples if this approach is to be used for quantitative analyses, such as assessing the size and MR properties (T_1, T_2, ADC, FA, etc.) of each tract (21,23).

In addition to producing noise and partial volume effects, manual ROI placement can be a major source of poor reproducibility in tractography. Compared to the one-ROI approaches, the two-ROI + BF approach is less sensitive to the ROI sizes and locations (Figs. 6 and 8). These results agree with the idea that the two ROIs impose strong anatomical constraints, and once a propagated line deviates from the path of interest, it is highly unlikely that the line will return to the path by chance. This robustness is exemplified in Fig. 8, in which rather large ROIs that encompass the AC are drawn but the reconstruction results are not affected. These results suggest that one can obtain highly reproducible results by establishing tracking protocols that wisely use anatomical features of the brain. For example, if two ROIs are defined in the right and left hemispheres (as in Fig. 8), the closest white matter tract that could share similar trajectories with the AC is the corpus callosum. In this case, the protocol should instruct the user to draw ROIs that are large enough to contain the entire AC and avoid including the corpus callosum. As long as these two anatomical criteria are fulfilled, reproducible results can be obtained.

CONCLUSIONS

We assessed the effects of noise and ROI size and location on DTI-based fiber reconstruction results for one-ROI and two-ROI + BF approaches using a postmortem rat brain dataset and Monte Carlo simulation. For the one-ROI approach, a small percentage (24–41%) of trajectories stayed inside the AC with SNR $\geq$ 20, and the percentage decreased with lower SNR. The two-ROI + BF approach led to valid trajectories regardless of the SNR, but the number of reconstructed lines decreased as the SNR declined. The two-ROI + BF approach also showed a low sensitivity to the ROI size and location. For studying prominent white matter tracts with known trajectories, it is highly beneficial to use the two-ROI + BF approach for reproducible reconstruction. However, when this technique is used for quantitative assessments, such as tract size, care must be taken because the number of reconstructed lines is sensitive to SNR.

REFERENCES

1. Basser PJ, Mattiello J, Le Bihan D. MR diffusion tensor spectroscopy and imaging. Biophys J 1994;66:259–267.
2. Moseley ME, Cohen Y, Kucharczyk J, Mintorovitch J, Asgari HS, Wendland MF, Tsuruda J, Norman D. Diffusion-weighted MR imaging of anisotropic water diffusion in cat central nervous system. Radiology 1990;176:439–445.
3. van Gelderen P, de Vleeschouwer MH, DesPres D, Pekar J, van Zijl PCM, Moonen CTW. Water diffusion and acute stroke. Magn Reson Med 1994;31:154–163.
4. Makris N, Worth AJ, Sorensen AG, Papadimitriou GM, Reese TG, Wedeen VJ, Davis TL, Stakes JW, Caviness VS, Kaplan E, Rosen BR, Pandya DN, Kennedy DN. Morphometry of in vivo human white matter association pathways with diffusion weighted magnetic resonance imaging. Ann Neurol 1997;42:951–962.
5. Pierpaoli C, Jezzard P, Basser PJ, Barnett A, Di Chiro G. Diffusion tensor MR imaging of human brain. Radiology 1996;201:637–648.
6. Henkelman R, Stanisz G, Kim J, Bronskill M. Anisotropy of NMR properties of tissues. Magn Reson Med 1994;32:592–601.
7. Beaulieu C, Allen PS. Determinants of anisotropic water diffusion in nerves. Magn Reson Med 1994;31:394–400.
8. Beaulieu C. The basis of anisotropic water diffusion in the nervous system—a technical review. NMR Biomed 2002;15:435–455.
9. Basser PJ, Jones DK. Diffusion-tensor MRI: theory, experimental design and data analysis—a technical review. NMR Biomed 2002;15:456–467.
10. Mori S, Crain BJ, Chacko VP, van Zijl PCM. Three dimensional tracking of axonal projections in the brain by magnetic resonance imaging. Ann Neurol 1999;45:265–269.
11. Xue R, van Zijl PCM, Crain BJ, Solaiyappan M, Mori S. In vivo three-dimensional reconstruction of rat brain axonal projections by diffusion tensor imaging. Magn Reson Med 1999;42:1123–1127.
12. Jones DK, Simmons A, Williams SC, Horsfield MA. Non-invasive assessment of axonal fiber connectivity in the human brain via diffusion tensor MRI. Magn Reson Med 1999;42:37–41.
13. Basser PJ, Pajevic S, Pierpaoli C, Duda J, Aldroubi A. In vitro fiber tractography using DT-MRI data. Magn Reson Med 2000;44:625–632.
14. Lazar M, Weinstein D, Hasan K, Alexander AL. Axon tractography with tensorlines. In: Proceedings of the 8th Annual Meeting of ISMRM, Denver, 2000. p 482.
15. Tuch DS, Belliveau JW, Wedeen V. A path integral approach to white matter tractography. In: Proceedings of the 8th Annual Meeting of ISMRM, Denver, 2000. p 791.
16. Conturo TE, Lori NF, Cull TS, Akbudak E, Snyder AZ, Shimony JS, McKinstry RC, Burton H, Raichle ME. Tracking neuronal fiber pathways in the living human brain. Proc Natl Acad Sci USA 1999;96:10422–10427.
17. Parker GJ. Tracing fiber tracts using fast marching. In: Proceedings of the 8th Annual Meeting of ISMRM, Denver, 2000. p 85.
18. Poupon C, Clark CA, Frouin V, Regis J, Bloch L, Le Bihan D, Mangin JF. Regularization of diffusion-based direction maps for the tracking of brain white matter fascicules. NeuroImage 2000;12:184–195.
19. Mori S, Van Zijl PC. Fiber tracking: principles and strategies—a technical review. NMR Biomed 2002;15:468–480.
20. Lori NF, Akbudak JS, Shimony TS, Snyder RK, Conturo TE. Diffusion tensor fiber tracking of brain connectivity: reliability analysis and biological results. NMR Biomed 2002;15:494–515.
21. Stieltjes B, Kaufmann WE, van Zijl PCM, Fredericksen K, Pearlson GD, Mori S. Diffusion tensor imaging and axonal tracking in the human brainstem. NeuroImage 2001;14:723–735.
22. Werring DJ, Toosy AT, Clark CA, Parker GJ, Barker GJ, Miller DH, Thompson AJ. Diffusion tensor imaging can detect and quantify corticospinal tract degeneration after stroke. J Neurol Neurosurg Psychiatry 2000;69:269–272.
23. Mori S, Kaufmann WE, Davatzikos C, Stieltjes B, Amodei L, Fredericksen K, Pearlson GD, Melhem ER, Solaiyappan M, Raymond GV, Moser HW, van Zijl PCM. Imaging cortical association tracts in human brain. Magn Reson Med 2002;47:215–223.
24. Catani M, Howard RJ, Pajevic S, Jones DK. Virtual in vivo interactive dissection of white matter fasciculi in the human brain. NeuroImage 2002;17:77–94.
25. Alexander DC, Pierpaoli C, Basser PJ, Gee JC. Spatial transformations of diffusion tensor magnetic resonance images. IEEE Trans Med Imaging 2001;20:1131–1139.
26. Xu D, Mori S, Solaiyappan M, van Zijl PC, Davatzikos C. A framework for callosal fiber distribution analysis. Neuroimage 2002;17:1131–1143.
27. Xu D, Mori S, Shen D, van Zijl PC, Davatzikos C. Spatial normalization of diffusion tensor fields. Magn Reson Med 2003;50:175–182.
28. Jones DK, Griffin LD, Alexander DC, Catani M, Horsfield MA, Howard R, Williams SC. Spatial normalization and averaging of diffusion tensor MRI data sets. Neuroimage 2002;17:592–617.
29. Lin CP, Tseng WY, Cheng HC, Chen JH. Validation of diffusion tensor magnetic resonance axonal fiber imaging with registered manganese-enhanced optic tracts. Neuroimage 2001;14:1035–1047.
30. Lazar M, Alexander AL. Error analysis of white matter tracking algorithms (streamlines and tensorlines) for DT-MRI. In: Proceedings of the 9th Annual Meeting of ISMRM, Glasgow, Scotland, 2001. p 506.
31. Lori NF, Akbuda E, Snyder AZ, Shimony JS, Conturo TE. Diffusion tensor tracking of human neuronal fiber bundles: simulation of effects of noise, voxel size and data interpolation. In: Proceedings of the 8th Annual Meeting of ISMRM, Denver, 2000. p 775.
32. Pierpaoli C, Basser PJ. Toward a quantitative assessment of diffusion anisotropy. Magn Reson Med 1996;36:893–906.